Hindawi Publishing Corporation
EURASIP Journal on Wireless Communications and Networking
Volume 2009, Article ID 879812, 14 pages
doi:10.1155/2009/879812

Research Article

Signal Classification in Fading Channels Using Cyclic Spectral Analysis

Eric Like,[1] Vasu D. Chakravarthy,[2] Paul Ratazzi,[3] and Zhiqiang Wu[4]

[1] *Air Force Institute of Technology, Department of Electrical Engineering, Wright-Patterson Air Force Base, OH 45433, USA*
[2] *Air Force Research Laboratory, Sensors Directorate, Wright-Patterson Air Force Base, OH 45433, USA*
[3] *Air Force Research Laboratory, Information Directorate, Griffiss Air Force Base, NY 13441, USA*
[4] *Department of Electrical Engineering, Wright State University, Dayton, OH 45435, USA*

Correspondence should be addressed to Zhiqiang Wu, zhiqiang.wu@wright.edu

Received 4 May 2009; Accepted 13 July 2009

Recommended by Mischa Dohler

Cognitive Radio (CR), a hierarchical Dynamic Spectrum Access (DSA) model, has been considered as a strong candidate for future communication systems improving spectrum efficiency utilizing unused spectrum of opportunity. However, to ensure the effectiveness of dynamic spectrum access, accurate signal classification in fading channels at low signal to noise ratio is essential. In this paper, a hierarchical cyclostationary-based classifier is proposed to reliably identify the signal type of a wide range of unknown signals. The proposed system assumes no a priori knowledge of critical signal statistics such as carrier frequency, carrier phase, or symbol rate. The system is designed with a multistage approach to minimize the number of samples required to make a classification decision while simultaneously ensuring the greatest reliability in the current and previous stages. The system performance is demonstrated in a variety of multipath fading channels, where several multiantenna-based combining schemes are implemented to exploit spatial diversity.

1. Introduction

Wireless access technologies have come a long way and are expected to radically improve the communication environment. On the other hand, the demand for spectrum usage in all environments has seen a considerable increase in the recent years. As a result, novel methods to maximize the use of the available spectrum have been proposed. One critical area is through the use of cognitive radio [1, 2]. Traditionally, wireless devices access the spectrum in a static bandwidth allocation. As the number of wireless users have increased, there has been a corresponding decrease in the amount of available spectrum. Cognitive radio seeks to relieve this burden by determining which areas of the spectrum are in use at a particular time. If a given band of the spectrum is not currently being used, that band could be used by another system. Given the dynamic nature of the current communication environment, cognitive radio and dynamic spectrum access has attracted strong interest in its capability of drastically increasing the spectrum efficiency. Many spectrum sensing algorithms have been proposed for cognitive radio, such as energy detection, pilot-based coherent detection, covariance-based detection, and cyclostationary detection [3, 4]. Cyclostationary detection-based spectrum sensing is capable of detecting the primary signal from the interference and noise even in very low SNR region [4]. Hence, the FCC has suggested cyclostationary detectors as a useful alternative to enhance the detection sensitivity in CR networks.

However, a more efficient method to maximize the use of the available spectrum would be to not simply avoid frequency bands that are in use, but rather to limit the amount of in-band transmission down to an acceptable low level so as to avoid interfering with the original user. For example, hybrid overlay/underlay waveforms have been proposed in [5] to exploit not only unused spectrum bands

but also under-used spectrum bands in cognitive radio. Since different signals are able to tolerate different amounts of interference, the signal type of the original user will have to be determined. In this case, merely detecting the presence of the signal will not be sufficient.

Modulation recognition and signal classification has been a subject of considerable research for over two decades. Classification schemes can generally be classified into one of two broad categories—likelihood-based (LB) approaches and feature-based (FB) approaches. LB approaches attempt to provide an optimal classifier by deriving a model for the signals being considered, and choosing the classification scheme with the greatest likelihood. However, a complete mathematical description of the model is usually extremely complex to arrive at, and generally the systems are highly sensitive to modeling errors. Additionally, the complexity of the classifier can frequently become too burdensome to operate in a real-time manner [6, 7].

FB approaches attempt to extract critical statistics from the received signal to make a classification based on the reduced data set. This can frequently be performed at a fraction of the complexity of LB systems. While FB methods are suboptimal in the Bayesian sense, they often provide near optimal performance [8].

FB systems have been implemented using a vast array of features. These have included statistics derived from the instantaneous amplitude, phase, and frequency, zero-crossing intervals, wavelet transforms, amplitude and phase histograms, constellation shapes, as well as many others [8–10]. However, many of these methods require a priori knowledge of critical signal statistics, such as the carrier frequency, carrier phase, symbol rate, or timing offset, among others. However, these statistics are generally unknown in practical applications, and requiring their knowledge severely limits the utility of the classifier.

One area that has demonstrated a considerable amount of potential is cyclostationary- (CS-) based approaches. CS methods have been demonstrated to be insensitive to unknown signal parameters and to preserve the phase information in the signal [11, 12]. In [13, 14] the Spectral Coherence Function (SOF) was used to classify lower-order digital modulation schemes. In [10], mixed second-order and fourth-order cyclic cumulants (CCs) were used to distinguish PSK and QAM signals. In [15] sixth- and lower-order CCs were utilized to classify a wide range of signals, and in [16] the ability of fourth-order through eighth-order CCs were investigated to classify QAM, ASK, and PSK signals of different orders.

However, each of the classifies above was only simulated in an AWGN channel and most assume knowledge of the unknown signal's carrier frequency, phase, or symbol rate. For a more realistic analysis, classifier performance should be assessed in fading channels. In [6] the authors investigated the use of eighth-order CCs to classify digital signals in a flat fading channel. By employing a multiantenna receiver using selection combining (SC), the system performance was shown to increase considerably. However, like the schemes above, it too assumed prior knowledge of the signal's symbol rate, and that the carrier frequency had already been removed. Additionally, while SC was shown to improve the performance of the classifier, it does not fully exploit the multiple received copies of the signal.

In this paper, we extend the results of [6, 14] to investigate the use of cyclic spectral analysis and CCs in a hierarchical approach for modulation recognition of a wide range of signals, with no a priori knowledge of the signal's carrier frequency, carrier phase, or symbol rate. Specifically, the proposed classifier will attempt to discriminate between AM, BFSK, OFDM, CDMA, 4-ASK, 8-ASK, BPSK, QPSK, 8-PSK, 16-PSK, 16-QAM, and 64-QAM modulation types. Multiple combining methods are investigated and the performance of the classifier under various channel conditions is assessed. The classifier features identified in [14] based on the SOF and in [6] based on eighth-order CCs are used as a benchmark for comparison purposes. In Section 2 the underlying statistics are developed, and the cyclostationary features to be used are defined. In Section 3 the multiantenna combining schemes to be investigated are described, and the proposed classifier design is given in Section 4. In Section 5 simulation results are presented, followed by a conclusion in Section 6.

2. Signal Statistic Development

2.1. Signal Model. A modulated signal as received by the classifier can be modeled as

$$\tilde{y}(t) = s(t - t_0)e^{j2\pi f_c t}e^{j\phi} + \tilde{n}(t), \tag{1}$$

where $\tilde{y}(t)$ is the complex-valued received signal, f_c is the carrier frequency, ϕ is the carrier phase, t_0 is the signal time offset, $n(t)$ is additive Gaussian noise, and $s(t)$ denotes the time-varying message signal. For digital signals, this can be further specified as

$$\tilde{y}(t) = e^{j2\pi f_c t}e^{j\phi}\sum_{k=-\infty}^{\infty} s_k p(t - kT_s - t_0) + \tilde{n}(t), \tag{2}$$

where $p(t)$ is the pulse shape, T_s is the symbol period, and s_k is the digital symbol transmitted at time $t \in (kT - T/2, kT + T/2)$. Here, the symbols s_k are assumed to be zero mean, identically distributed random variables.

CS-based features have been used in numerous ways as a reliable tool to determine the modulation scheme of unknown signals [10, 14, 16]. CS-based approaches are based on the fact that communications signals are not accurately described as stationary, but rather more appropriately modeled as cyclostationary. While stationary signals have statistics that remain constant in time, the statistics of CS signals vary periodically. These periodicities occur for signals of interest in well defined manners due to underlying periodicities such as sampling, scanning, modulating, multiplexing, and coding. This resulting periodic nature of signals can be exploited to determine the modulation scheme of the unknown signal.

2.2. Second-Order Cyclic Features. The autocorrelation function of a CS signal $x(t)$ can be expressed in terms of its Fourier Series components [11, 12]:

$$R_x(t,\tau) = E\{x(t+\tau/2)x^*(t-\tau/2)\} = \sum_{\{\alpha\}} R_x^\alpha(\tau)e^{j2\pi\alpha t}, \quad (3)$$

where $E\{\cdot\}$ is the expectation operator, $\{\alpha\}$ is the set of Fourier components, and the function $R_x^\alpha(\tau)$ giving the Fourier components is termed the cyclic autocorrelation function (CAF) given by

$$R_x^\alpha(\tau) = \lim_{T\to\infty} 1/T \int_{-T/2}^{T/2} R_x(t,\tau)e^{-j2\pi\alpha t}. \quad (4)$$

Alternatively, in the case when $R_x(t,\tau)$ is periodic in t with period T_0, (4) can be expressed as

$$R_x^\alpha(\tau) = 1/T_0 \int_{-T_0/2}^{T_0/2} R_x(t,\tau)e^{-j2\pi\alpha t}. \quad (5)$$

The Fourier Transform of the CAF, denoted the Spectral Correlation Function (SCF), is given by

$$S_x^\alpha(f) = \int_{-\infty}^{\infty} R_x^\alpha(\tau)e^{-j2\pi f\tau}d\tau. \quad (6)$$

This can be shown to be equivalent (assuming cyclo-ergodicity) to [11]

$$S_X^\alpha(f) = \lim_{T\to\infty}\lim_{\Delta t\to\infty}\frac{1}{\Delta t}\int_{-\Delta t/2}^{\Delta t/2}\frac{1}{T}X_T\left(t,f+\frac{\alpha}{2}\right)X_T^*\left(t,f-\frac{\alpha}{2}\right)dt, \quad (7)$$

$$X_T(t,f) = \int_{t-T/2}^{t+T/2} x(u)e^{j2\pi f u}du. \quad (8)$$

Here it can be seen that S_x^α is in fact a true measure of the correlation between the spectral components of $x(t)$. A significant benefit of the SCF is its insensitivity to additive noise. Since the spectral components of white noise are uncorrelated, it does not contribute to the resulting SCF for any value of $\alpha \neq 0$. This is even the case when the noise power exceeds the signal power, where the signal would be undetectable using a simple energy detector. At $\alpha = 0$, where noise is observed, the SCF reduces to the ordinary Power Spectral Density (PSD).

To derive a normalized version of the SCF, the Spectral Coherence Function (SOF) is given as

$$C_X^\alpha(f) = \frac{S_X^\alpha(f)}{\left[S_X^0(f+\alpha/2)^* S_X^0(f-\alpha/2)\right]^{1/2}}. \quad (9)$$

The SOF is seen to be a proper coherence value with a magnitude in the range of $[0, 1]$. To account for the unknown phase of the SOF, the absolute value of $C_X^\alpha(f)$ is computed and used for classification. The SOFs of some typical modulation schemes are shown in Figures 1 and 2. The SOF of each modulation scheme generates a highly distinct image. These images can then be used as spectral fingerprints to identify the modulation scheme of the received signal.

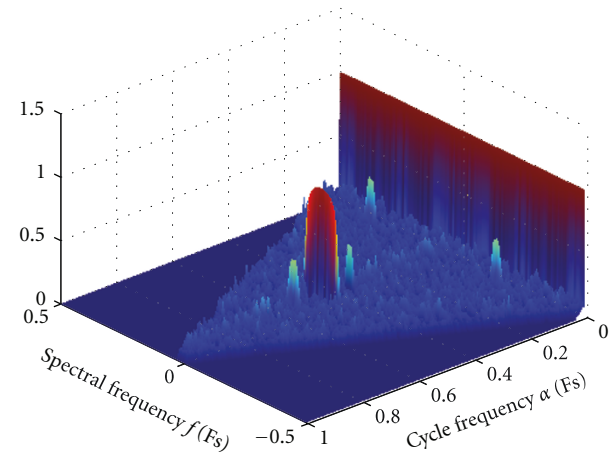

Figure 1: SOF of a BPSK signal in an AWGN Channel at 5 dB SNR, with 1/Ts = Fs/10, Fc = 0.25 Fs, no. of samples = 4096.

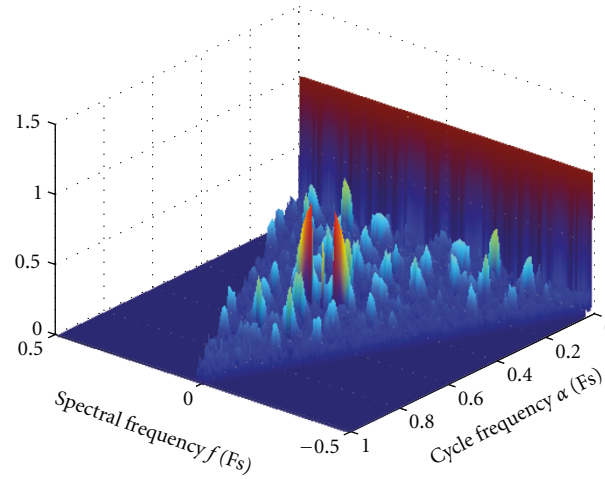

Figure 2: SOF of a BFSK signal in an AWGN Channel at 5 dB SNR, with 1/Ts = Fs/10, Fc = 0.25 Fs, no. of samples = 4096.

An additional benefit to using the SOF is its insensitivity to channel effects. Wireless signals are typically subject to severe multipath distortion. Taking this into consideration, the SCF of a received signal is given as

$$S_Y^\alpha(f) = H\left(f+\frac{\alpha}{2}\right)H^*\left(f-\frac{\alpha}{2}\right)S_x^\alpha(f), \quad (10)$$

$$y(t) = x(t)\otimes h(t), \quad (11)$$

where $h(t)$ is the unknown channel response, and $H(f)$ is the Fourier Transform of $h(t)$. Here it can be seen that the resulting SCF of the received signal can be significantly distorted depending on the channel. However, when forming the SOF, by substituting (10) into (9) it is evident that the channel effects are removed, and the resulting SOF is equal to that of the original undistorted signal [12]. As a result, the SOF is preserved as a reliable feature for identification even when considering propagation through multipath channels, so long as no frequency of the signal of interest is completely

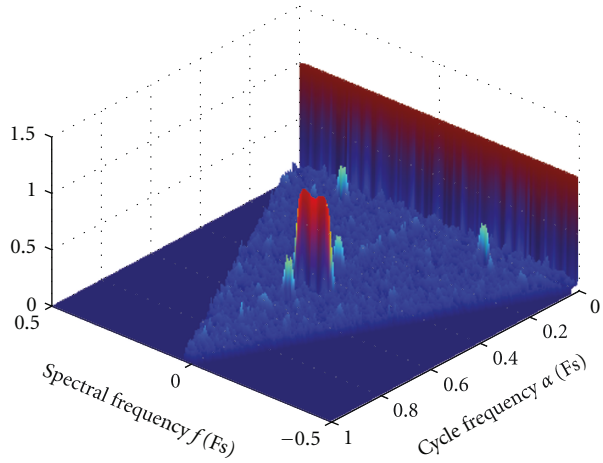

Figure 3: SOF of a BPSK signal in a Multipath Fading Channel at 5 dB SNR, with 1/Ts = Fs/10, Fc = 0.25 Fs, no. of samples = 4096.

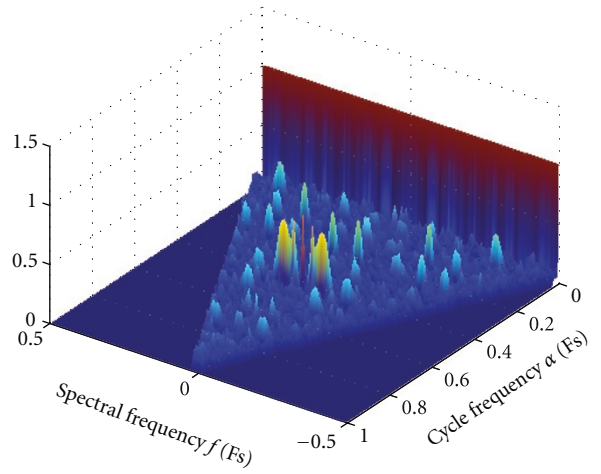

Figure 4: SOF of a BFSK signal in a Multipath Fading Channel at 5 dB SNR, with 1/Ts = Fs/10, Fc = 0.25 Fs, no. of samples = 4096.

nullified by the channel. The SOFs of some typical signals undergoing multipath fading are shown in Figures 3 and 4.

To compute the SOF for a sampled signal, a sliding windowed FFT of length N can be used to compute X_T, and a sum taken over the now discrete versions of X_T gives the resulting equation for $S_X^\alpha(f)$. Additionally, the limits in (7) and (8) must be made finite, and an estimate of the SCF is obtained. This has the effect of limiting the temporal and spectral resolution of the SCF. In (7), Δt is the amount of time over which the spectral components are correlated. This limits the temporal resolution of the signal to Δt. In [17] the cyclic resolution is shown to be approximately $\Delta\alpha = 1/\Delta t$. Similarly, the spectral resolution is limited to $\Delta f = 1/T$, where $1/T$ is the resolution of the FFT used to compute X_T.

To obtain a reliable estimate of the SCF, the random fluctuations of the signal must be averaged out. The resulting requirement is that the time-frequency resolution product must be made very large, with $\Delta t \Delta f \gg 1$, or equivalently, $\Delta f \gg \Delta\alpha$. This has the effect of requiring a much finer resolution for the cycle frequencies than would be provided by the FFT operation. To compensate for this, it has been proposed to zero pad the input to the FFTs out to the full length of the original signal [14]. However, this leads to a computationally infeasible task. A more suitable method is to first estimate the cycle frequencies of interest using the method outlined in [18]. After the appropriate cycle frequencies have been located, the SCF can be computed using the equivalent method of frequency smoothing on the reduced amount of data:

$$S_X^\alpha(f) = \frac{1}{\Delta f}\int_{f-\Delta f/2}^{f+\Delta f/2} X_{\Delta t}\left(t, f+\frac{\alpha}{2}\right) X_{\Delta t}^*\left(t, f-\frac{\alpha}{2}\right) dt, \quad (12)$$

where $X_{\Delta t}(t, f)$ is defined in (8) with T replaced by Δt.

The resulting feature derived from the SOF is a three-dimensional image. This presents an unreasonable amount of data for a classifier to operate on in real time. Therefore, it must be further reduced to provide a more computationally manageable feature. In [14] the authors proposed using merely the cycle frequency profile of the SOF. However, in our previous work of [13] it was demonstrated that with a minimal increase in computational complexity, both the frequency profile as well as the cycle frequency profile can be used, creating a pseudo-three-dimensional image of the SOF which performs at a significantly higher degree of reliability for classification. The resulting feature used for classification is then defined as the cycle frequency profile:

$$\vec{\alpha} = \max_f [C_X^\alpha] \quad (13)$$

and the spectral frequency profile

$$\vec{f} = \max_\alpha [C_X^\alpha]. \quad (14)$$

These features can then be analyzed using a pattern recognition-based approach. Due to its ease of implementation, and its ability to generalize to any carrier frequency or symbol rate, a neural network-based system is proposed to process the feature vectors. This system will be outlined in Section 4.

2.3. Higher-Order Cyclic Features. While the SOF produces highly distinct images for different modulation schemes, some modulation schemes (such as different orders of a single modulation scheme) produce identical images. Therefore, while the SOF is able to reliably classify each of the analog signals as well as classify the digital schemes into a modulation family, it will not be able to distinguish between some digital schemes (namely, QAM and M-PSK, $M > 4$), or determine the order of the modulation. As an example of this, compare the estimated SOF of the BPSK signal in Figure 1 with that of a 4-ASK signal shown in Figure 5.

To discriminate between signals of these types, higher-order cyclic statistics (HOCSs) must be employed. For this end, we introduce the nth-order/q-conjugate temporal moment function:

$$R_x(t, \boldsymbol{\tau})_{n,q} = E\left\{\prod_{i=1}^{i=n} x^{(*)_i}(t+\tau_i)\right\}, \quad (15)$$

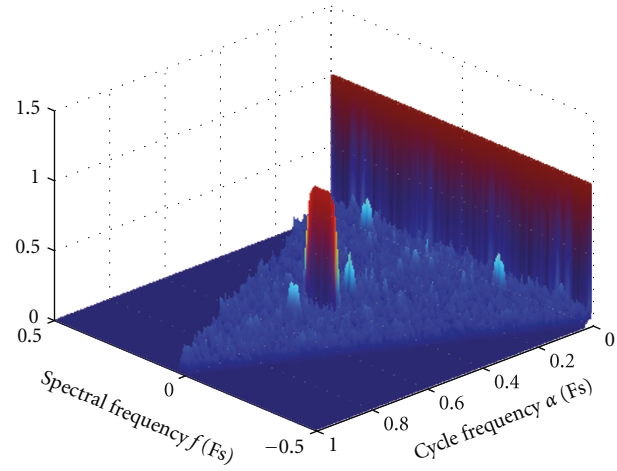

FIGURE 5: SOF of a 4-ASK signal in an AWGN Channel at 5 dB SNR, with 1/Ts = Fs/10, Fc = 0.25 Fs, no. of samples = 4096.

where $(*)$ represents the one of q total conjugations. For the case of $n = 2$, $q = 1$, $\tau_1 = \tau/2$, and $\tau_2 = -\tau/2$, the TMF reduces to the autocorrelation function defined in (3). Like the autocorrelation function, the TMF of CS signals exhibits one or more periodicities and can be expressed in terms of its Fourier coefficients:

$$R_x(t,\boldsymbol{\tau})_{n,q} = \sum_{\{\alpha\}} R_x^{\alpha}(\boldsymbol{\tau})_{n,q} e^{j2\pi\alpha t},$$
$$R_x^{\alpha}(\boldsymbol{\tau})_{n,q} = \lim_{T\to\infty} 1/T \int_{-T/2}^{T/2} R_x(t,\boldsymbol{\tau})_{n,q} e^{-j2\pi\alpha t}, \tag{16}$$

where $R_x^{\alpha}(\boldsymbol{\tau})_{n,q}$ is termed the cyclic temporal moment function.

To isolate the cyclic features present at an order n from those made up of products of lower-order features we make use of the nth-order/q-conjugate temporal cumulant (TC). The TC is given by the moment to cumulant formula

$$C_x(t,\boldsymbol{\tau})_{n,q} = \mathrm{Cum}\left\{x^{(*)_1}(t+\tau_1)\cdots x^{(*)_n}(t+\tau_n)\right\}$$
$$= \sum_{\{P_n\}} (-1)^{Z-1}(Z-1)! \prod_{z=1}^{Z} m_x(t,\boldsymbol{\tau}_z)_{n_z,q_z}, \tag{17}$$

where $\{P_n\}$ is the set of distinct partitions of $\{1,2,\ldots,n\}$, τ_z is a delay vector with indices specified by z, and n_z and q_z correspond to the number of elements and the number of conjugated terms in the subset P_z, respectively. When computing the TC, the effect of lower-order moments is effectively subtracted off, leaving the only remaining impact due to the current order. The TC is also a periodic function for cyclostationary signals, with its Fourier components given by

$$C_x^{\gamma}(\boldsymbol{\tau})_{n,q} = \lim_{T\to\infty} 1/T \int_{-T/2}^{T/2} C_x(t,\boldsymbol{\tau})_{n,q} e^{-j2\pi\gamma t}, \tag{18}$$

where $C_x^{\gamma}(\boldsymbol{\tau})$ is the cyclic cumulant (CC) of $x(t)$.

Since it is computationally infeasible to perform a multi-dimensional Fourier Transform of (18) to compute a higher-order variation of the SCF, we are restricted to manipulate (18) directly as a feature for classification. However, by substituting (2) into (17) and (18), it can be shown that the resulting value of the CC is given by [6]

$$C_x^{\gamma}(\boldsymbol{\tau})_{n,q} = C_{s,n,q} T_s^{-1} e^{-j2\pi\beta t_0} e^{j(n-2q)\phi} e^{j2\pi f_c \sum_{u=1}^{n-1}(-)_u \tau_u}$$
$$\times \int_{-\infty}^{\infty} p^{(*)_n}(t) \prod_{u=1}^{u=n-1} p^{(*)_n}(t+\tau_u) e^{-j2\pi\beta} dt, \tag{19}$$
$$\gamma = \beta + (n-2q) f_c, \quad \beta = \frac{k}{T_s},$$

where $C_{s,n,q}$ is the nth-order/q-conjugate cumulant of the stationary discrete data sequence, and the possible minus sign, $(-)_u$, comes from one of the q conjugations $(*)_n$. Thus, the resulting value of the CC of the received signal is directly proportional to $C_{s,n,q}$. The value of $C_{s,n,q}$ is well known for common modulation schemes and is given in Table 1 [6].

As in the case of the SOF, the magnitude of (19) is taken to remove the phase dependence on the carrier frequency, phase, and signal time offset. The resulting feature is given as

$$\Gamma_y(\gamma,\boldsymbol{\tau})_{n,q} = \left| C_{s,n,q} T_s^{-1} \right.$$
$$\left. \times \int_{-\infty}^{\infty} p^{(*)_n}(t) \prod_{u=1}^{u=n-1} p^{(*)_n}(t+\tau_u) e^{-j2\pi\beta} dt \right|,$$
$$\gamma = \beta + (n-2q) f_c, \quad \beta = \frac{k}{T_s}. \tag{20}$$

Assuming a raised cosine pulse shape, the maximum of the resulting function $\Gamma_y(\gamma,\boldsymbol{\tau})_{n,q}$ has been shown to occur at $\boldsymbol{\tau} = \vec{\mathbf{0}}_{\mathbf{n}}$, where $\vec{\mathbf{0}}_{\mathbf{n}}$ is an n-dimensional zero vector. Furthermore, at $\boldsymbol{\tau} = \vec{\mathbf{0}}_{\mathbf{n}}$, the function decreases with increasing k [6]. k is therefore chosen to be 1 to maximize the test statistic. $\Gamma_y(\gamma,\boldsymbol{\tau})_{n,q}$ should then be evaluated at $\gamma = 1/T_s + (n-2q) f_c$.

The desired value of γ used to evaluate the CC depends on both f_c and $1/T_s$, which are both unknown and will need to be estimated. This value of γ can be derived by noting that cyclic features will only occur at intervals of $1/T_s$. For a raised cosine pulse, the magnitude of $\Gamma_y(\gamma,\boldsymbol{\tau})_{n,q}$ obtains its largest value at $k = 0$, corresponding to a cycle frequency of $\gamma = (n-2q) f_c$. The next largest peak occurs at $k = 1$, which is the desired cycle frequency. To estimate the desired value of γ, all that is needed is to search for the cycle frequency corresponding to the largest cyclic feature, and evaluate the CC at an offset of $1/T_s$ from this location. Given that the variance of the CC estimates increase with increasing order [16], we desire to use the lowest order CC possible to estimate $1/T_s$ to achieve a more reliable estimate. The second-order/one-conjugate CC is therefore selected to estimate $1/T_s$, as all of the modulation schemes

Table 1: Theoretical stationary cumulants [6].

$C_{s,n,q}$	4-ASK	8-ASK	BPSK	Q-PSK
$C_{s,2,0}$	1	1	1	0
$C_{s,2,1}$	1	1	1	1
$C_{s,4,0}$	−1.36	−1.24	−2	1
$C_{s,4,1}$	−1.36	−1.24	−2	0
$C_{s,4,2}$	−1.36	−1.24	−2	−1
$C_{s,6,0}$	8.32	7.19	16	0
$C_{s,6,1}$	8.32	7.19	16	-4
$C_{s,6,2}$	8.32	7.19	16	0
$C_{s,6,3}$	8.32	7.19	16	4
$C_{s,8,0}$	−111.85	−92.02	−272	−34
$C_{s,8,1}$	−111.85	−92.02	−272	0
$C_{s,8,2}$	−111.85	−92.02	−272	34
$C_{s,8,3}$	−111.85	−92.02	−272	0
$C_{s,8,4}$	−111.85	−92.02	−272	−34
$C_{s,n,q}$	8-PSK	16-PSK	16-QAM	64-QAM
$C_{s,2,0}$	0	0	0	0
$C_{s,2,1}$	1	1	1	1
$C_{s,4,0}$	0	0	−0.68	−0.62
$C_{s,4,1}$	0	0	0	0
$C_{s,4,2}$	−1	−1	−0.68	−0.62
$C_{s,6,0}$	0	0	0	0
$C_{s,6,1}$	0	0	2.08	1.80
$C_{s,6,2}$	0	0	0	0
$C_{s,6,3}$	4	4	2.08	1.80
$C_{s,8,0}$	1	0	−13.98	−11.50
$C_{s,8,1}$	0	0	0	0
$C_{s,8,2}$	0	0	−13.98	−11.50
$C_{s,8,3}$	0	0	0	0
$C_{s,8,4}$	−33	−33	−13.98	−11.50

being considered will contain a feature at this cycle frequency. Using the value of $\gamma = 1/T_s$ computed from the second-order CC, paired with the estimate of $\gamma = (n - 2q) f_c$ obtained for each CC, the computation of the value of $\gamma = 1/T_s + (n-2q) f_c$ is straightforward.

The resulting values of the different order/conjugate pairs of the CCs can now be used to classify the signal further to discriminate between signals for which the SOF was unable. By referring to Table 1, the specific modulation type as well as its order can be determined from the expected values of $C_{s,n,q}$. In [6] it was proposed to use only the eighth-order CCs of the received signal. However, the results can be improved by using the lower-order CCs in the estimate, whose variance is shown to be less than that of corresponding higher orders. By implementing a hierarchical scheme, lower-order CCs can perform an initial classification, followed by progressively higher-order CCs to further refine the classification decision. In this way a more reliable estimate can be obtained. Furthermore, in poor channel conditions, the hierarchical scheme is expected to better distinguish between modulation families than a scheme based purely on a single-higher order CC, due to the lower variance in the CCs.

2.4. Identification of OFDM Signals. In an OFDM system, the subcarriers can be appropriately modeled as independently modulated signals which exhibit their own second-order cyclostationary statistics (SOCSs). However, the fact that their bandwidths overlap reduces the total amount of observed spectral coherence (SOF) due to the "destructive interference" between the overlapping cyclostationary features. As the length of the cyclic prefix used in the OFDM system is shortened, the observed features in the SOF are also decreased. In the case where an OFDM signal is generated without a cyclic prefix, the remaining cyclostationary features are severely diminished [19]. While research has shown that cyclostationary features can be artificially introduced into a transmitted OFDM signal by transmitting correlated data on selected subcarriers [20], in the absence of these intentionally designed phenomena the cyclic features present in a received OFDM signal will

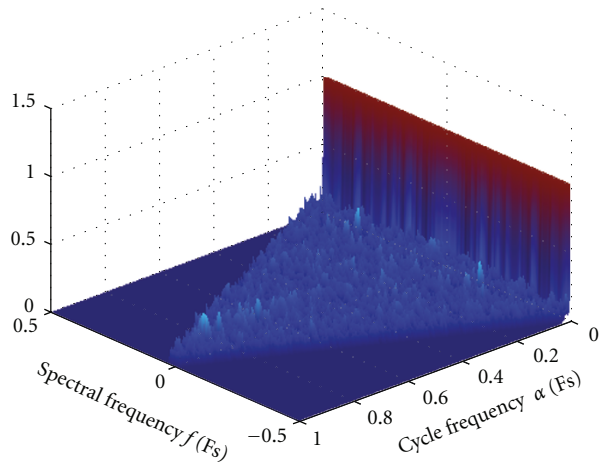

Figure 6: SOF of a QPSK signal in an AWGN Channel at low (0 dB) SNR, with 1/Ts = Fs/10, Fc = 0.25 Fs, no. of samples = 4096.

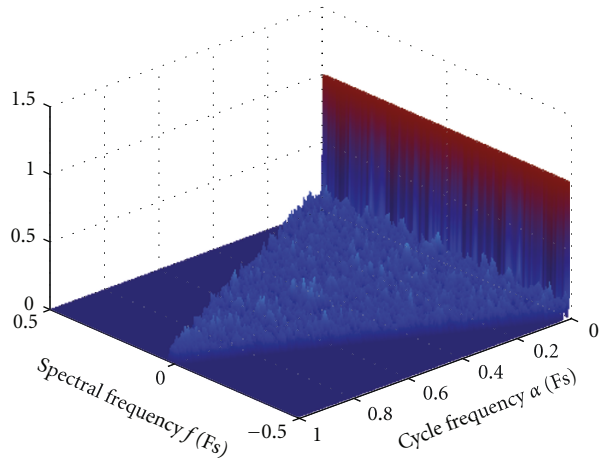

Figure 7: SOF of an OFDM signal in an AWGN Channel at low (0 dB) SNR, with 32 subcarriers, subcarrier spacing ΔF = Fs/10, Fc = 0.25 Fs, no. of samples = 4096.

generally be very weak and difficult to detect. In the presence of low SNR, the difference between the SOF of OFDM signals with no cyclic prefix and that of single carrier QAM and MPSK signals ($M > 2$) becomes negligible. As an example, refer to Figures 6 and 7 depicting the SOF of a QPSK signal and OFDM signal, respectively, generated at an SNR of 0 dB.

While the existence of cyclic prefix in OFDM signal makes the detection and classification of OFDM signal much easier, in reality the signal detector/classifier sometimes needs to make decision in a short observation time window. When this observation window is shorter than the duration of one OFDM symbol, cyclic prefix is not included in the observation window. Hence, since there are numerous efficient algorithms to detect and classify an OFDM signal based on its cyclic prefix through the use of a simple autocorrelation procedure [21–23], we focus on the case of an OFDM signal transmitted with no cyclic prefix. Therefore, an intermediate stage is needed between the SOF-based classifications and the HOCS-based classifications.

A simple yet effective method to distinguish OFDM signals from the single carrier signals in question is obtained by considering the fact that OFDM signals are composed of multiple independently time varying signals. By use of the Central Limit Theorem from probability theory, these can be approximated as a Gaussian random signal [21]. Through the use of a simple Gaussianity test, the OFDM signals can therefore be accurately identified. Since Gaussian signals do not exhibit features for CCs other than their 2nd-order/1-conjugate CC, the CC features derived above to distinguish between the HOCS features can also be used to classify an OFDM signal, assuming the number of subcarriers present is high.

3. Multiantenna Combining

In the presence of multipath fading channels, the received signal can be severely distorted. Several methods exist to exploit spacial diversity through the use of multiple receiver antennas. By assuming that the channel fades independently on each antenna, the signal received on each can be combined in various ways to improve performance. The general equation for the received analytic signal undergoing multipath propagation is given by

$$\tilde{y}(t) = \sum_{p=1}^{P} \kappa_p e^{j\theta_p} \tilde{x}\left(t - t_p\right) + \tilde{n}(t), \tag{21}$$

where $\kappa_p e^{\theta_p}$ is the channel response on path p, t_p is the delay of the pth path, and P is the total number of paths received by the classifier.

This can be separated into two general situations. In the first situation, the channel is varying sufficiently slowly so that it can be assumed to be static over the block of data being analyzed.

If the signal is assumed to only be experiencing flat fading, the simplest combining method is to employ a selection combiner (SC). In [6], the effectiveness of an SC-based system was evaluated to combat the effects of flat fading for modulation recognition. By estimating the received power on each antenna, the signal on the antenna with the highest observed power can be selected for classification, while the others are discarded. When assuming that the noise on each antenna has identical powers, this choice will correspond to the signal with the largest SNR, which leads to an extremely simple implementation.

However, in the case of flat fading, a maximum ratio combiner (MRC) can also be implemented. In this case, the signal received from each antenna is weighted by its SNR before being summed with the signals from the other antennas. In practice, the value of the SNR can be estimated simply by using one of several methods [24–26]. However, for the signals to combine coherently, the unknown phase on each channel must be compensated for before adding

them together. This can be performed by computing the correlation between signals from two channels given by

$$E\{\tilde{y}_1(t)\tilde{y}_2^*(t)\} = E\Big\{\Big(\kappa_1 e^{j\theta_1}\tilde{x}(t) + \tilde{n}_1(t)\Big) \times \Big(\kappa_2^* e^{-j\theta_2}\tilde{x}^*(t) + \tilde{n}_2^*(t)\Big)\Big\} = \sigma_{\tilde{x}}^2 \kappa_1 \kappa_2 e^{j(\theta_1-\theta_2)}, \quad (22)$$

where $\sigma_{\tilde{x}}^2$ is the power of the signal to be classified. From here, the relative phase difference is given as the phase of the resulting statistic:

$$\Delta\hat{\theta} = \angle\Big(\sigma_{\tilde{x}}^2 \kappa_1 \kappa_2 e^{j(\theta_1-\theta 2)}\Big). \quad (23)$$

The signal $\tilde{y}_2(t)$ can then be multiplied by $e^{j\Delta\hat{\theta}}$ to align its phase with the phase of the first channel. This procedure can be repeated as necessary depending on the number of antennas employed.

An additional method to compensate for channel corruption in the SOF computation is through a variant of the MRC. While the SOF was derived to be highly insensitive to channel distortion in (10), the SOF image obtained when a deep fade can be significantly distorted by the additive noise components present, which will be amplified when forming the SOF from the SCF. The MRC variant described here then attempts to compensate for this effect by combining weighted estimates of the SOF from each receiver. For this method, the SOF is computed independently for the signal received on each antenna. After the feature vectors $\vec{\alpha}$ and $\vec{f}$ are formed, they are each weighted by the SNR estimated on their respective antennas. Then each is summed, and the procedure follows as before. It is worth noting that this method can be utilized in any fading channel, without the necessity for the assumption of a flat fading channel.

The second general situation exists when the channel is not varying slow enough to be approximated as static throughout the signal's evaluation. Since each of the classification methods above attempts to estimate expected values of joint moments, they are quickly corrupted by a rapidly fading channel. The HOCS features are particularly sensitive since they require a greater amount of samples to converge, during which time the channel can vary drastically. The first stage SOF-based classifier is less sensitive to channel variations, thus providing greater incentive for its use as the first stage in the system.

4. Classifier Design

The proposed classifier is designed to classify AM, BFSK, OFDM, DS-CDMA, 4-ASK, 8-ASK, BPSK, QPSK, 8-PSK, 16-PSK, 16-QAM, and 64-QAM modulation types. It is designed in a hierarchical approach to classify the signals using the smallest amount of required data possible, while simultaneously maximizing the reliability of the system. At each stage in the system, the signal's modulation scheme is either classified or grouped with similar schemes narrowed down into a smaller subset. The system is designed to require no knowledge of the received signal's carrier frequency, phase shift, or symbol rate, and only assumes that the signal's presence has been identified, and that it is located within the bandwidth of interest.

The first stage of the classifier computes the SOF of the signal by (i) using the SSCA method outlined in [18] to estimate the cycle frequencies of interest, (ii) applying (12) followed by (9) to compute the SOF of the received signal, and (iii) compressing the data into the feature vector composed of the concatenation of $\vec{\alpha}$ and $\vec{f}$. As mentioned in Section 2.2, the feature vector is analyzed by a neural network-based system. Neural networks were chosen due to their relative ease of setup and use as well as its ability to generalize to any carrier frequency or symbol rate. The system consists of five independent neural networks, each trained to classify a signal as either AM, BFSK, DS-CDMA, or a linear modulation scheme with a real-valued constellation (BPSK, 4-ASK, 8-ASK) or a complex-valued constellation (OFDM, 8-PSK, 16-PSK, 16-QAM, 64-QAM). Each network has four neurons in their hidden layer and one neuron in the output layer, each layer with a hyperbolic tangent sigmoid transfer function. The inputs to each network are the concatenated profile vectors. A system diagram for this first stage is given in Figure 8.

The BPSK and ASK signals demonstrate identical SOF images and are not distinguishable based on that metric alone. Similarly, the PSK and QAM signals have identical spectral components. As mentioned in the previous section, the OFDM signal is composed of potentially independently varying signals on each subchannel, which may or may not demonstrate SOCS. However, due to the overlapping nature of the subchannels in an OFDM system, the resulting SOF is decreased, resulting in an SOF image that resembles those of QAM and PSK signals. Additionally, the DS-CDMA scheme can be thought to look like a BPSK signal. However, due to the underlying periodicities incurred by both its symbol rate as well as its spreading code, it produces features not found in BPSK or QPSK signals. Thus it can be reliably classified by its SOF image without knowledge of its spreading code.

The HOCS-based processing is also implemented in a hierarchical approach to maximize the ability to accurately determine the class of a signal before further narrowing the list of candidate modulations. This is a critical step since the variance of the CC estimates increases with increasing order [16]. Therefore, we attempt to classify a signal using the lowest order CC possible before proceeding to higher-order CCs.

In each stage, the feature vector used for classification is composed of the appropriate CCs estimated from the received signal:

$$\hat{\Psi} = \left[\Gamma_y\left(\frac{1}{T}, \vec{\mathbf{0}}_{\mathbf{n}}\right)_{n,q_1}, \ldots, \Gamma_y\left(\frac{1}{T}, \vec{\mathbf{0}}_{\mathbf{n}}\right)_{n,q_k}\right], \quad (24)$$

where n and q_j refer to the appropriate order and number of conjugations for the stage. This vector is then compared

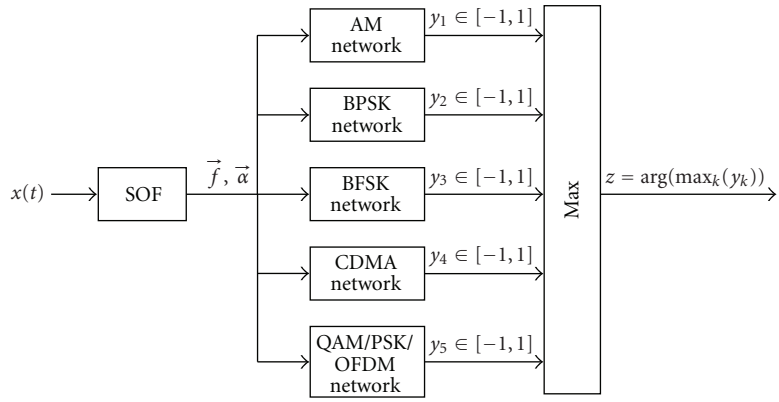

Figure 8: SOF system diagram.

to the expected vector obtained for each modulation type, defined similarly as

$$\Psi^{(i)} = \left[\Gamma^{(i)}\left(\frac{1}{T}, \vec{\mathbf{0}}_{\mathbf{n}}\right)_{n,q_1}, \ldots, \Gamma^{(i)}\left(\frac{1}{T}, \vec{\mathbf{0}}_{\mathbf{n}}\right)_{n,q_k}\right], \quad (25)$$

where i corresponds to one of the M possible modulation schemes being considered by the current stage. The class corresponding to the feature vector with the minimum Euclidean distance from the estimated vector is selected. The processing is then handed off to the next stage until the final modulation scheme as been determined.

The network diagram of the system is shown in Figure 9. If the SOF network determined the signal to have a real-valued modulation scheme (BPSK, 4-ASK, 8-ASK), then it is handed off to the final classification stage using eighth-order CCs. Otherwise, the fourth-order CCs are used to classify the signal as being an OFDM signal or as having either a circular constellation (8-PSK, 16-PSK) or a square constellation (QPSK, 16-QAM, 62-QAM). For each signal class, the final stage of the classifier forms the feature vector $\hat{\Psi}$ from the five eighth-order CCs of the received signal, except for OFDM signals which were already identified using fourth-order CCs.

5. Simulation Results

Simulations were run with AM, BFSK, OFDM, DS-CDMA, 4-ASK, 8-ASK, BPSK, QPSK, 8-PSK, 16-PSK, 16-QAM, and 64-QAM modulated signals. Each of the digital signals was simulated with an IF carrier frequency uniformly distributed between 0.23 and 0.27 times the sampling rate, a symbol rate uniformly distributed between 0.16 and 0.24 times the sampling rate, and a raised cosine pulse shape with a 50% excess bandwidth, with the exception of the BFSK which was modeled with a rectangular pulse shaping filter. The OFDM signal employed 32 subcarriers using BPSK modulation (without a cyclic prefix), and like the other digital signals was passed through a raised cosine filter with a 50% excess bandwidth. The analog signals were also bandlimited using the same raised cosine filter. Additionally, the classifier's receive filter is assumed to be an ideal low-pass filter. Since the symbol rate is assumed to be unknown, the digital signals were not sampled at an integer multiple of the symbol rates, but were sampled at a constant rate independent of the symbol rate and the IF carrier frequency.

The first stage of the classifier used 4096 received time samples, corresponding to an average of approximately 410 symbols, to compute the SOF estimate of the signal, and used this estimate in the neural-network system. The HOCS-based system was tested with 65 536 samples for its classification decision, corresponding to an average of approximately 6500 symbols. The system was tested in a variety of channel conditions, with an SNR range of 0 dB to 15 dB. The channel models simulated include a flat fading channel, two-path fading channel, and a harsh 20-path fading channel. Each of the fading channels implemented used independent equal-power paths with Rayleigh distributed amplitudes and uniformly distributed phases. The channels are simulated for two distinct fading scenarios:

(1) slow fading such that the channel can be approximated as constant over the block of observed data;

(2) fast fading with each path maintaining a coherence value of 0.9 over 500 samples, approximately equal to 50 symbols.

Additionally, it is assumed that the SNR of the signal on each antenna can be accurately estimated, and that the channel phase offset between antennas is accurately determined for the slow flat fading channel.

The system performance is measured by its probability of correct classification (Pcc), defined as the percentage of the total number of modulation classifications made that were accurate. The SOF-based classifier from [14] using only the cycle frequency profile is simulated as a benchmark for comparison to the first stage of the proposed classifier. This demonstrates the advantage of using both the cycle frequency as well as the spectral frequency profile for the initial classification stage. The purely eighth-order CC feature vector from [6] is used as a benchmark for comparison to the proposed classifier from end to end. However, to achieve a fair comparison, the AM, DS-CDMA, and BFSK signals were

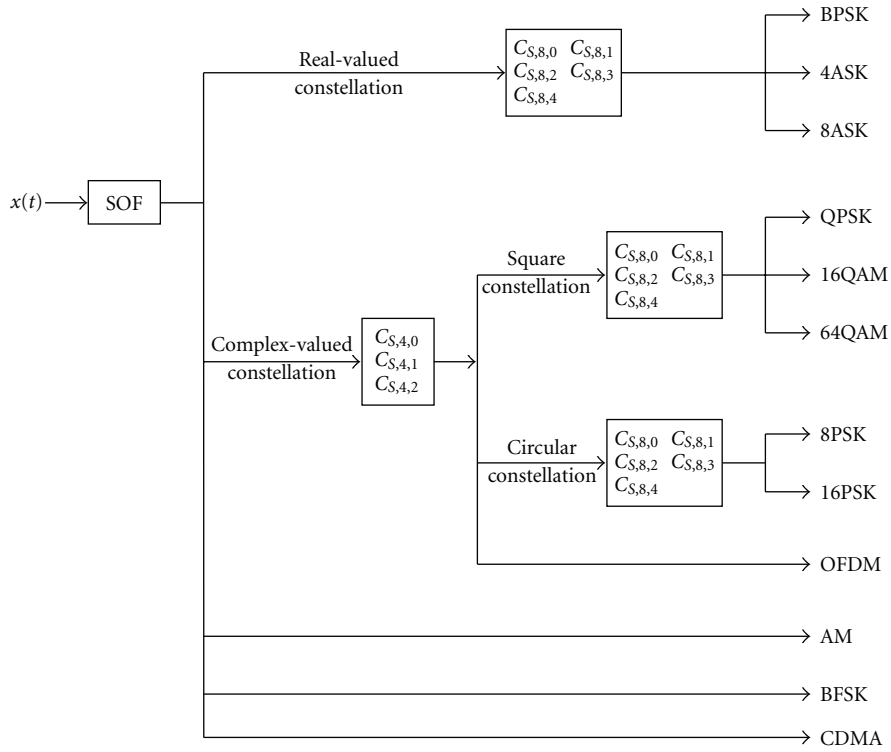

Figure 9: Proposed system diagram.

excluded from consideration for this case since the purely eighth-order CC does not have the ability to classify signals of this type.

The systems were first tested in a slow flat fading channel. Here, the systems were simulated using a multiantenna approach. The initial SOF-based stage used the MRC-variant method outlined in Section 3, while the HOCS-based stage utilized traditional MRC. Figure 10 compares the performance of the first stage of the proposed classifier with that of its benchmark. As can be readily seen, the proposed classifier obtains a significant performance increase over the baseline. The initial stage of the proposed classifier achieves the remarkably high rate nearly 100% Pcc for all SNR levels of interest when using four antennas with the MRC variant. Figure 11 compares the final classification performance of the proposed classifier to its eighth-order CC counterpart. In this case, the proposed classifier achieves a gain of 3 dB SNR over the benchmark. It is also noteworthy that as pointed out in [6], with the addition of only a single antenna, a considerable performance gain is achieved.

Next, the systems were tested in a two path as well as a 20-path slow fading channel. As mentioned earlier, the fading channel is assumed to be static over the duration of the observation. Here, the initial SOF-based stage was again implemented with the MRC variant, while the HOCS-based systems used SC. The performance of the initial classification stage subject to the two-path channel is shown in Figure 12 and the results under the 20-path channel are shown in Figure 13. These figures demonstrate the robustness of the SOF against multipath channel effects, as it is subject to only a slight performance degradation as compared to the flat fading channel.

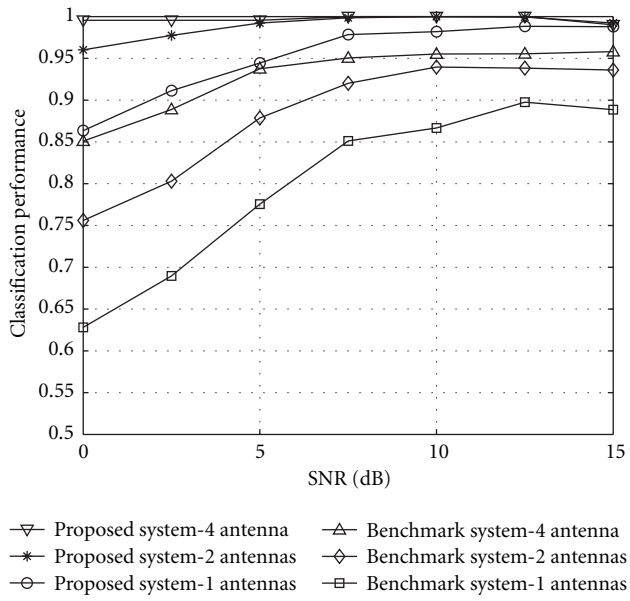

Figure 10: Classification performance of proposed initial SOF-based classification stage and benchmark in a slow flat fading channel using the MRC-variant combining scheme.

The performance of the final classification decision is shown in Figure 14 for the two-path case and in Figure 15

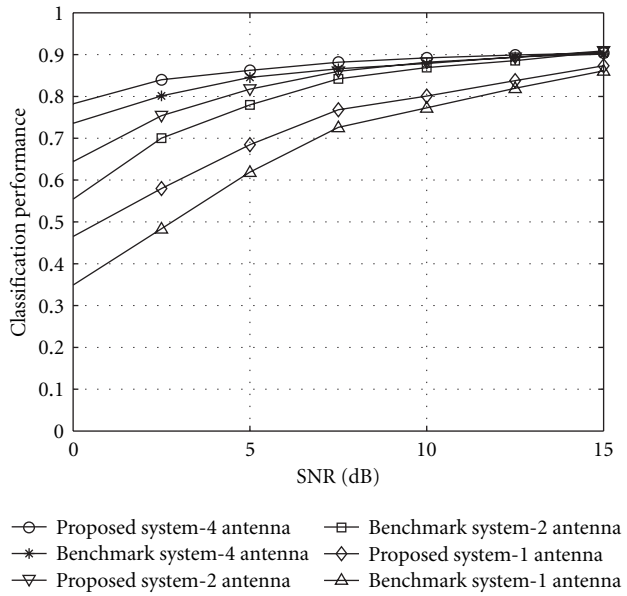

Figure 11: Final classification performance of proposed classifier and benchmark in a slow flat fading channel using MRC.

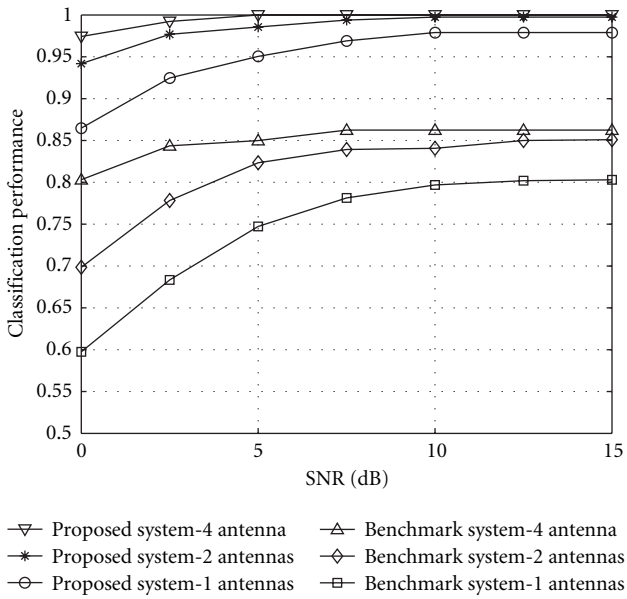

Figure 12: Classification performance of proposed initial SOF-based classification stage and benchmark in a slow two-path fading channel using the MRC-variant combining scheme.

for the multipath case. The performance of each system is significantly degraded from the performance under the flat fading channel. The performance is insufficient to classify a signal with any reasonable degree of reliability. However, a benefit to the multistage approach is that it utilizes lower-order CCs in each decision stage, thus lowering the variance of the estimated statistic. While this does not achieve a significant benefit in the final classification stage, it does allow for a more reliable estimate of the family of the signal. This is demonstrated in Figures 16 and 17 where the

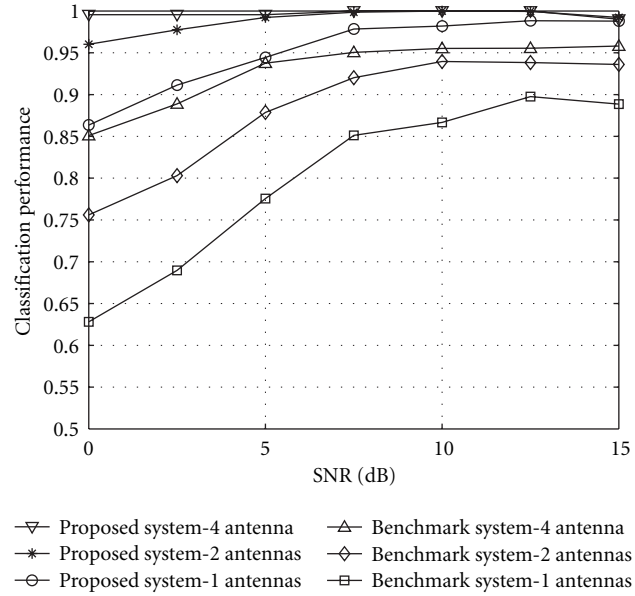

Figure 13: Classification performance of proposed initial SOF-based classification stage and benchmark in a slow 20-path fading channel using the MRC-variant combining scheme.

ability of the two systems to classify the received signal as having a real-valued constellation (BPSK, 4ASK, or 8ASK), a square-constellation (QPSK, 16QAM, or 64 QAM), a circular constellation (8PSK or 16PSK), or as being an OFDM signal, where the other three signal types are not considered as the purely eighth-order CC feature vector is not capable of classifying them. Here, while it is noted that the number of antennas used does not affect the overall modulation-family classification performance, using the multistage approach does increase the observed classification performance by approximately two to three times.

Finally, the classifier performance was evaluated under the faster fading channels. The performance of the SOF-based classifier is given in Figures 18 and 19. Again, this initial stage of the classifier is only moderately degraded. Furthermore, while each classifier is unable to reliably determine the exact modulation scheme of the received signal under these harsh channel conditions, the multistage approach is still able to reliably determine the modulation family of the signal of interest. The system performance under the fast varying flat and 20-path channels are shown in Figures 20 and 21.

The ability of the system to still achieve a high degree of reliability in determining the modulation family is in part due to the insensitivity of the SOF to the multipath affect as well as to the fewer number of required symbols that must be observed before a classification can be made. Since this stage of the classifier requires significantly fewer observed symbols to make a classification, it is only moderately affected. While the purely eighth-order CC-based classifier is drastically degraded, the proposed classifier is still able to produce a moderate gain in modulation class recognition, demonstrating the ability of the lower-order cumulants to

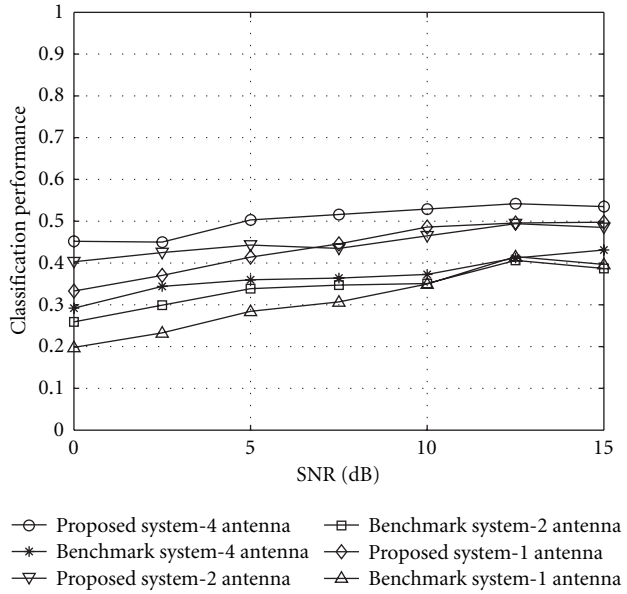

Figure 14: Final classification performance of proposed classifier and benchmark in a slow two-path fading channel using SC.

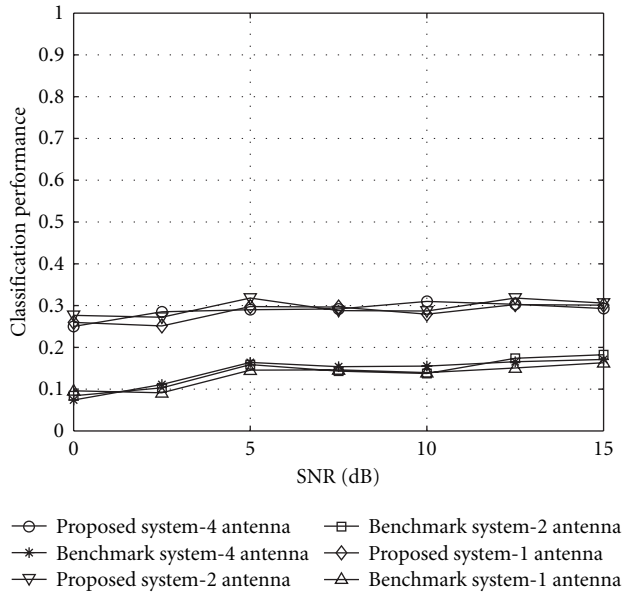

Figure 15: Final classification performance of proposed classifier and benchmark in a slow 20-path fading channel using SC.

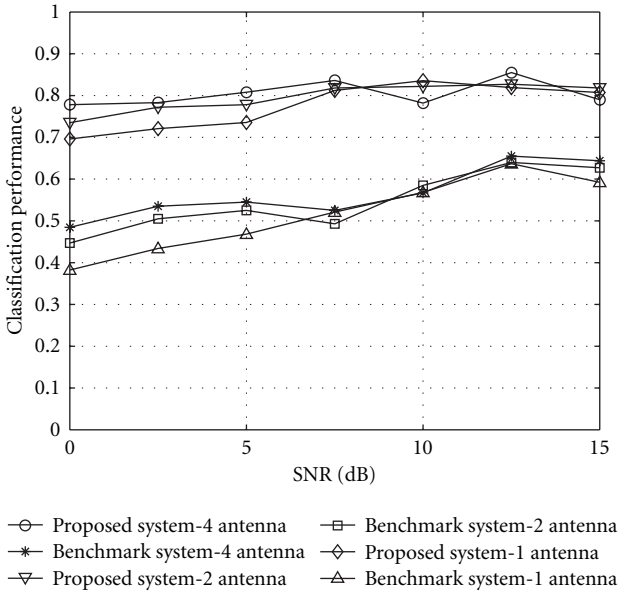

Figure 16: Ability of proposed classifier and benchmark to determine a signal's modulation family in a slow two-path fading channel using SC.

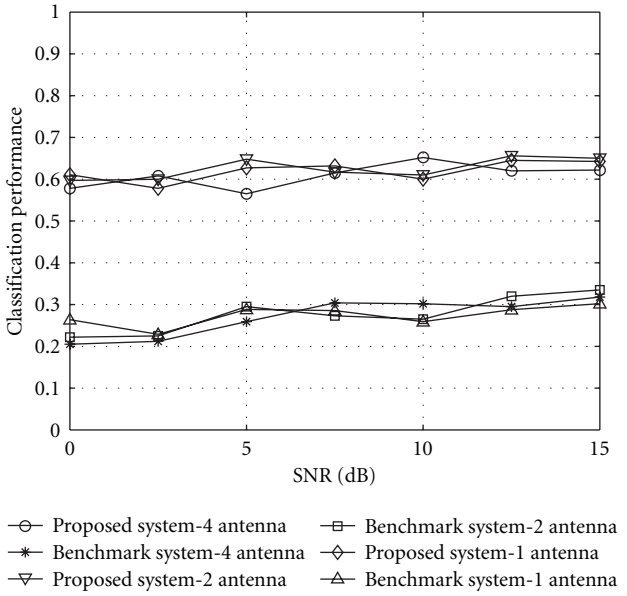

Figure 17: Ability of proposed classifier and benchmark to determine a signal's modulation family in a slow 20-path fading channel using SC.

reliably distinguish between lower order modulations even in the presence of multipath fading.

6. Conclusion

In this paper, a hierarchical modulation recognition system is proposed to classify a wide range of signals. The classifier leverages the ability of cyclic spectral analysis and cyclic cumulants (CCs) to distinguish between signals while requiring no a priori knowledge of critical signal statistics, such as carrier frequency, carrier phase, and symbol rate. By using lower-order cyclic statistics to make initial classifications, followed by higher-order cyclic statistics to further refine the decision, the classifier is able to obtain a higher overall classification rate. Through the use of several multiantenna combining methods, the performance of the classifier is further improved in multipath fading channels, both when the channel is varying slowly enough so that can be assumed

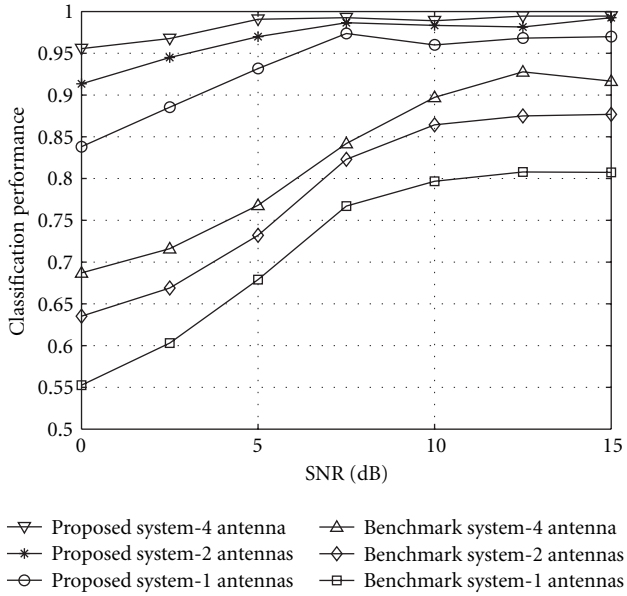

Figure 18: Classification performance of proposed initial SOF-based classification stage and benchmark in a faster varying flat fading channel with using the MRC-variant combining scheme.

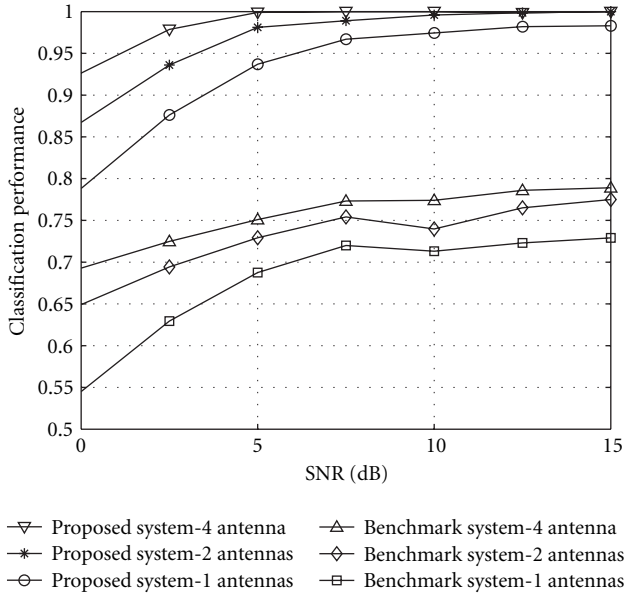

Figure 19: Classification performance of proposed initial SOF-based classification stage and benchmark in a faster varying 20-path fading channel using the MRC-variant combining scheme.

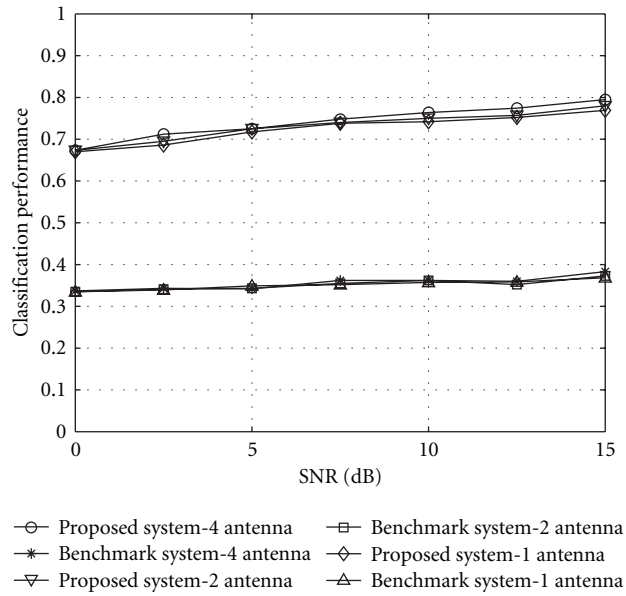

Figure 20: Ability of proposed classifier and benchmark to determine a signal's modulation family in a faster varying flat fading channel using SC.

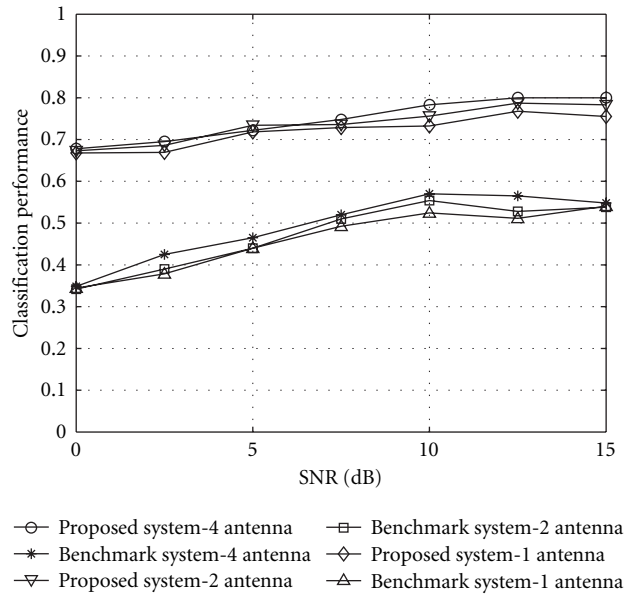

Figure 21: Ability of proposed classifier and benchmark to determine a signal's modulation family in a faster varying 20-path fading channel using SC.

to be static during the period of observation as well when it is fading more rapidly.

Acknowledgments

This paper is based upon work supported by the Dayton Area Graduate Studies Institute (DAGSI), National Science Foundation under Grants no. 0708469, no. 0737297, no. 0837677, the Wright Center for Sensor System Engineering, and the Air Force Research Laboratory. Any opinions, findings, and conclusions, or recommendations expressed in this paper are those of the authors and do not necessarily reflect the views of the funding agencies.

References

[1] J. Mitola, *Cognitive radio: an integrated agent architecture for software defined radio*, Ph.D. dissertation, KTH Royal Institute of Technology, Stockholm, Sweden, 2000.

[2] *Proceedings of the 1st IEEE International Symposium on New Frontiers in Dynamic Spectrum Access Networks*, Baltimore, Md, USA, 2005.

[3] J. Ma, G. Y. Li, and B. H. Juang, "Signal processing in cognitive radio," *Proceedings of the IEEE*, vol. 97, no. 5, pp. 805–823, 2009.

[4] S. Haykin, D. J. Thomson, and J. H. Reed, "Spectrum sensing for cognitive radio," *Proceedings of the IEEE*, vol. 97, no. 5, pp. 849–877, 2009.

[5] V. Chakravarthy, Z. Wu, M. A. Temple, F. Garber, R. Kannan, and A. Vasilakos, "Novel overlay/underlay cognitive radio waveforms using SD-SMSE framework to enhance spectrum efficiency - part I: theoretical framework and analysis in AWGN channel," *IEEE Transactions on Communications*, vol. 57, no. 12, 2009.

[6] O. A. Dobre, A. Abdi, Y. Bar-Ness, and W. Su, "Selection combining for modulation recognition in fading channels," in *Proceedings of IEEE Military Communications Conference (MILCOM '05)*, Atlatnic City, NJ, USA, October 2005.

[7] A. Swami and B. Sadler, "Hierarchical digital modulation classification using cumulants," *IEEE Transactions on Communication*, vol. 48, no. 3, pp. 416–429, 2000.

[8] O. A. Dobre, A. Abdi, Y. Bar-Ness, and W. Su, "Survey of automatic modulation classification techniques: classical approaches and new trends," *IET Communications*, vol. 1, no. 2, pp. 137–156, 2007.

[9] E. Azzouz and A. Nandi, *Automatic Modulation Recognition of Communication Signals*, Kluwer Academic Publishers, Dordrecht, The Netherlands, 1996.

[10] P. Marchard, J. Lacoume, and C. Martret, "Multiple hypothesis modulation classification based on cyclic cumulants of different orders," in *Proceedings of IEEE International Conference on Acoustics, Speech, and Signal Processing (ICASSP '98)*, vol. 4, pp. 2157–2160, Seattle, Wash, USA, May 1998.

[11] W. A. Gardner, W. A. Brown, and C.-K. Chen, "Spectral correlation of modulated signals—part II: digital modulation," *IEEE Transactions on Communications*, vol. 35, no. 6, pp. 595–601, 1987.

[12] W. A. Gardner, *Cyclostationarity in Communications and Signal Processing*, IEEE Press, Piscataway, NJ, USA, 1993.

[13] E. Like, V. Chakravarthy, and Z. Wu, "Reliable modulation classification at low SNR using spectral correlation," in *Proceedings of the 4th Annual IEEE Consumer Communications and Networking Conference (CCNC '07)*, pp. 1134–1138, 2007.

[14] A. Fehske, J. Gaeddert, and J. H. Reed, "A new approach to signal classification using spectral correlation and neural networks," in *Proceedings of the 1st IEEE International Symposium on New Frontiers in Dynamic Spectrum Access Networks (DySPAN '05)*, pp. 144–150, Baltimore, Md, USA, 2005.

[15] C. M. Spooner, "On the utility of sixth-order cyclic cumulants for RF signal classification," in *Proceedings of the 35th Asilomar Conference on Signals, Systems and Computers*, vol. 1, pp. 890–897, Pacific Grove, Calif, USA, November 2001.

[16] O. A. Dobre, Y. Bar-Ness, and W. Su, "Higher-order cyclic cumulants for high order modulation classification," in *Proceedings of IEEE Military Communications Conference (MILCOM '03)*, vol. 1, pp. 112–117, Monterey, Calif, USA, October 2003.

[17] W. A. Gardner, "Measurement of spectral correlation," *IEEE Transactions on Acoustics, Speech, and Signal Processing*, vol. 34, no. 5, pp. 1111–1123, 1986.

[18] R. S. Roberts, W. A. Brown, and H. H. Loomis Jr., "Computationally efficient algorithms for cyclic spectral analysis," *IEEE Signal Processing Magazine*, vol. 8, no. 2, pp. 38–49, 1991.

[19] D. Vucic, M. Obradovic, and D. Obradovic, "Spectral correlation of OFDM signals related to their PLC applications," in *Proceedings of IEEE International Symposium on Power-Line Communications and Its Applications (ISPLC '02)*, Athens, Greece, March 2002.

[20] P. D. Sutton, K. E. Nolan, and L. E. Doyle, "Cyclostationary signatures for rendezvous in OFDM-based dynamic spectrum access networks," in *Proceedings of the 2nd IEEE International Symposium on New Frontiers in Dynamic Spectrum Access Networks (DySPAN '07)*, pp. 220–231, Dublin, Ireland, 2007.

[21] N. Han, G. Zheng, S. H. Sohn, and J. M. Kim, "Cyclic autocorrelation based blind OFDM detection and identification for cognitive radio," in *Proceedings of the 4th International Conference on Wireless Communications, Networking and Mobile Computing (WiCOM '08)*, 2008.

[22] A. Bouzegzi, P. Jallon, and P. Ciblat, "A second order statistics based algorithm for blind recognition of OFDM based systems," in *Proceedings of IEEE Global Telecommunications Conference (GLOBECOM '08)*, pp. 3257–3261, New Orleans, La, USA, 2008.

[23] H. Li, Y. Bar-Ness, A. Abdi, O. S. Somekh, and W. Su, "OFDM modulation classification and parameters extraction," in *Proceedings of the 1st International Conference on Cognitive Radio Oriented Wireless Networks and Communications (CROWNCOM '06)*, 2006.

[24] D. Pauluzzi and N. Beaulieu, "A comparison of SNR estimation techniques for the AWGN channel," in *Proceedings of IEEE Pacific Rim Conference on Communications, Computers, and Signal Processing*, 1995.

[25] Z. Chen, B. Nowrouzian, and C. J. Zarowski, "An investigation of SNR estimation techniques based on uniform Cramer-Rao lower bound," in *Proceedings of the 48th Midwest Symposium on Circuits and Systems (MWSCAS '05)*, vol. 1, pp. 215–218, August 2005.

[26] A. Wiesel, J. Goldberg, and H. Messer-Yaron, "SNR estimation in time-varying fading channels," *IEEE Transactions on Communications*, vol. 54, no. 5, pp. 841–848, 2006.